CDF/ANAL/EXOTIC/CDFR/7589
Version 0.04
September 6, 2005

$Z^0 \to \tau\tau$ Cross-Section Measurement

S. Baroiant,[a] M. Chertok,[a] T. Kamon,[b] V. Khotilovich,[b] R. Lander,[a]
A. Safonov[a1]

(a) University of California, Davis
(b) Texas A&M University

Abstract

In this note we present a measurement of the $Z \to \tau\tau$ cross-section in the channel with one hadronically decaying tau and the other tau decaying electronically. This measurement is based on 349 pb^{-1} of Run II data and updates previous result described in CDF Note 6552. The measured cross-section is $\sigma(p\bar{p} \to Z)Br(Z \to \tau\tau) = 265 \pm 20(stat) \pm 21(syst) \pm 15(lumi)$ pb in agreement with the NLO prediction.

[1]For questions or comments, please email safonov@fnal.gov

Contents

1 Introduction

In Run II the τ physics plays an important role in both electroweak measurements and searches for new phenomena. For the latter case, both Higgs and Supersymmetry phenomenology predict tau enriched detector signatures.

This signal is a testing ground for detector performance and offline software validation, but more importantly it also serves as a "calibration" for a number of other analyses: R_p-violating $\tilde{t}_1$ and lepto-quark searches, SM and SUSY Higgs and doubly charged Higgs/Higgsino decaying to taus, $t\bar{t}$, high $\tan\beta$ mSUGRA. A well measured $Z^0 \to \tau\tau$ cross-section ensures that tau identification is robust and well understood leading to improved systematic uncertainties in the future analyses.

In this note, we follow the method described in CDF note 6552[1] with several improvements aimed at better precision of the measurement. Minor changes in tau identification show better signal efficiency and background rejection. As a result of optimization, we found that that previously used thresholds on momenta of the two leptons are appropriate. Using $\not\!\!E_T$ corrected for lepton and tau energy mismeasurement has provided better separation of the signal and W+jets background, and re-optimized event topolgy cuts improve signal selection efficiency. Overall, we have somewhat larger amount of backgrounds compared to previous measurement; nevertheless the optimized procedure improves precision of this measurement.

2 Analysis Outline

This analysis is based on 349 pb^{-1} of Run II data. We measure the cross-section of the $p\bar{p} \to Z \to \tau\tau$ process in a mode with one electron decaying into an electron and the other one decaying into hadrons. We study kinematical and geometrical acceptance of the signal events, electron and tau identification efficiencies and select a sample of candidate events. Then a set of event topology cuts is applied to suppress major backgrounds. Backgrounds are estimated using a combination of data driven and MC based techniques followed by an iterative procedure that allows statistical separation of signal from major backgrounds: QCD (characterized by poor electron isolation), $\gamma +$ *jet* (better fake lepton isolation, symmetric in charge) EWK events with two real leptons, and W+jet backgrounds (large transverse mass of the electron and $\not\!\!E_T$). We use this procedure to extract the rate of the signal events and convert it into the cross-section measurement.

3 Data

3.1 Data and Monte Carlo Samples

This analysis uses the *etlp0d* dataset reconstructed with offline version 5.3.1 and reprocessed with appropriate patches. We select events collected by the electron+track trigger [3].

At Level 1, the trigger requires a single tower with EM $E_T \geq 8$ GeV and a matching XFT track with $P_T \geq 8$ GeV. At Level 2, these requirements are re-applied using Level 2 clusters. Also, a matching CES cluster with pulse hight corresponding to electron $E_T > 3$ GeV/c is required. At Level 2, there is an additional requirement that the second XFT track with $P_T \geq 5$ GeV exists and is separated from the electron candidate by at least 10 degrees in ϕ. At Level 3, the trigger requires a reconstructed 8 GeV loose electron candidate and an *isolated* track (*seed*) with $P_T \geq 5$ GeV, with the *isolation* defined as a

requirement that there be no tracks with $P_T \geq 1.5$ GeV in the annulus $0.17 < \Delta R < 0.52$ around the *seed* track. Further details can be found in [3]. We use several Monte Carlo (MC) samples produced in 5.3.3 (except $Z \to ee$ in 5.3.2); all samples except $t\bar{t}$ have extra min-bias events overlayed:

- Inclusive $Z/\gamma^* \to \tau_e\tau_h$ Pythia (*zewk*8*t*)
- Inclusive $W \to e\nu$ Pythia (*wewkae*)
- Inclusive $W \to \tau\nu \to e\nu\nu$ Pythia (*wewk*9*t*)
- Inclusive $Z/\gamma^* \to ee$ Pythia (*zewkae*)
- Inclusive $t\bar{t}$ Herwig (*ttop*0*z*)

3.2 Luminosity Measurement

We use the *goodrun_em_nosi_v*7 list and the integrated luminosity was calculated using actual run sections in the dataset. The obtained value is 349 pb^{-1}and we assign a standard 5.8% systematic uncertainty. We keep luminosity uncertainty separate from other systematics.

4 Event Selection

4.1 Kinematical and Geometrical Acceptance

We select events with at least one electron candidate with $E_T^e > 10$ GeV and at least one tau candidate with $p_T^\tau > 15$ GeV$/c$, where p_T^τ is calculated using reconstructed track and π^0 information with appropriate corrections [1]. The two have to be separated in the $\eta - \phi$ plane by $\Delta R > 0.7$ and satisfy certain fiducial requirements. The latter is needed to ensure high and well understood efficiency of triggerring and robust event reconstruction. These selections determine the kinematical and geometrical acceptance for this measurement. A full list of requirements is in Table 3.

4.2 Lepton Identification

To improve the purity of the signal, a set of electron and tau identification requirements is applied. We then remove likely $Z \to ee$ and conversion electron candidates. To further minimize backgrounds, we require events to pass additional event-level cuts designed to suppress QCD and W+jet backgrounds.

Electron identification cuts (excluding isolation) are based on the standard requirements, e.g. see [4], and are listed in Table 5. Having considered several choices for isolation, e.g. see [1], we decided to use track-based isolation, I^e_{trk}, defined in the $\eta - \phi$ plane as:

$$I^{e\,\Delta R}_{trk} = \sum_{\Delta R < 0.4} p_T \ , \tag{1}$$

where summatiuon runs over all tracks in $\eta - \phi$ cone of size $\Delta R < 0.4$ around the electron track. Each track must satisfy $|z_0^{e-trk} - z_0^{trk}| < 5$ cm and have at least two segments in axial and stereo superlayers of five or more hits each. We later estimate QCD background contamination using the shape of the electron tracking

$\lvert\Delta(\cot\theta)\rvert \leq 0.04$
$\Delta S_{xy} \leq 0.2$ cm

Table 1: Requirements for a pair of tracks to be tagged as a conversion. S_{xy} is defined as the distance between the two track trajectory helices at the point of their closest approach to each other.

	Calorimeter based:
Second cluster:	$E_T^{EM} \geq 8$ GeV
	$(E^{had}/E^{EM}) \leq 0.12$
	opposite charge
	$76 \leq M(e^+, e^-) \leq 106$ GeV
	Track based:
Second Track:	trk = defTrack
	$p_T \geq 10$ GeV/c
	$I_{trk}^{e,\Delta R} \leq 2.0$ GeV/c
	opposite charge
	$66 \leq M(e-trk, trk) \leq 111$ GeV

Table 2: $Z \to ee$ veto definition.

isolation distribution, therefore, to avoid biases, we do not apply calorimeter isolation cuts. Instead, to improve background rejection, we use π^0 isolation defined as

$$I_{\pi^0}^{e\,\Delta R} = \sum_{0.22<\Delta R<0.4} p_T^{\pi^0}\,, \tag{2}$$

where we only use good 2D-reconstructed π^0's.

Tau identification cuts used in this study follow our previous measurement [1] and are listed in Table 6.

4.3 Event Topology Cuts

We apply several cuts to suppress backgrounds. The largest background for $Z \to \tau\tau$ is QCD jet production (including heavy flavor) that enters the sample via one of the jets faking an electron, while the other jet fakes a hadronic tau. There are several other process contributing to the backgrounds, but one of them, W+jet, is rather large and is particularly difficult to estimate. It passes event selection via the real electron coming from W decay and the jet faking a hadronic tau.

We start by removing "technical" backgrounds. First, we remove events with an electron tagged as a conversion, definied as in Table 1. The second step is to remove the Drell-Yan background. We do this by eliminating events satisfying the requirements outlined in Table 2.

The next step is to suppress backgrounds using knowledge of the kinematical properties of the signal and background events. This step requires optimization and is described in detail later in the paper.

CEM Cluster:	$E_T^{EM} > 10$ GeV
	wedges with I_η =16 and 35 excluded
Matching Track:	$p_T^{e-trk} > 8$ GeV/c
	$\lvert z_0^{e-trk}\rvert < 60$ cm
	$\lvert z_{R=137}^{e-trk}\rvert < 150$ cm
	$9 < \lvert z_{R_{CES}}^{e-trk}\rvert < 230$ cm
	$\lvert x_{R_{CES}}^{e-trk}\rvert < 21.5$ cm
Tau cluster:	$p_T^{\tau} > 15$ GeV/c
	$\lvert \eta_{det}^{\tau}\rvert < 1.0$
Seed Track:	$p_T^{\tau-trk} > 6$ GeV/c
	$\lvert z_{R=137}^{\tau-trk}\rvert < 150$ cm
	$9 < \lvert z_{R_{CES}}^{\tau-trk}\rvert < 230$ cm
$\Delta R(e,\tau) > 0.7$	

Table 3: Acceptance definition.

5 Geometrical and Kinematical Acceptance

For consistency with the measurement of the $p\bar{p} \to Z$ cross-section in the electron and muon channels ([6]), we measure the cross-section of the $p\bar{p} \to Z/\gamma^* \to \tau\tau$ process under the constraint that the true invariant mass of the di-tau system is within a window

$$66\ \text{GeV}/c^2 < M_{\tau\tau} < 116\ \text{GeV}/c^2 \tag{3}$$

Accordingly, we define the acceptance as the fraction of $Z^0/\gamma^* \to \tau_e\tau_h$ events produced within the mass window $66 < M_{\tau\tau} < 116$ GeV/c^2 with at least one electron and one tau candidate[2] in the central part of the detector.

The electron candidate is required to have a reconstructed track with $p_T > 8$ GeV/c fully contained in the fiducial volume of the COT to match trigger XFT requirements and the extrapolated position of the track at the CES radius has to satisfy CES fiduciality requirements. For the tau candidate, the seed track is required to have $p_T > 6$ GeV/c and satisfy XFT and CES fiduciality requirements. Electron and tau candidates have to be separated in $\eta - \phi$ space by $\Delta R > 0.7$. Detailed selections are listed in Table 3.

Acceptance is calculated using a Pythia MC and the following formula:

$$\alpha_0 = \frac{N_{evt}^{pass\ acceptance\ reqs}}{N_{evt}^{generated}[66 < M_{\tau\tau} < 116\ \text{GeV}/c^2]}, \tag{4}$$

where $N_{event}^{generated}$ is the total number of $Z^0/\gamma^* \to \tau_e\tau_h$ events generated and falling in the mass range $66 < M_{\tau\tau} < 116$ GeV/c^2, where $M_{\tau\tau}$ is calculated using generator level information, and $N_{event}^{acceptance}$ is the number of events passing acceptance requirements (listed in Table 3).

5.1 Scale Factors and Systematic Uncertainties

Here we discuss corrections and systematic uncertainties in the measurement of the acceptance.

[2]Reconstructed leptons are required to match the generator level leptons

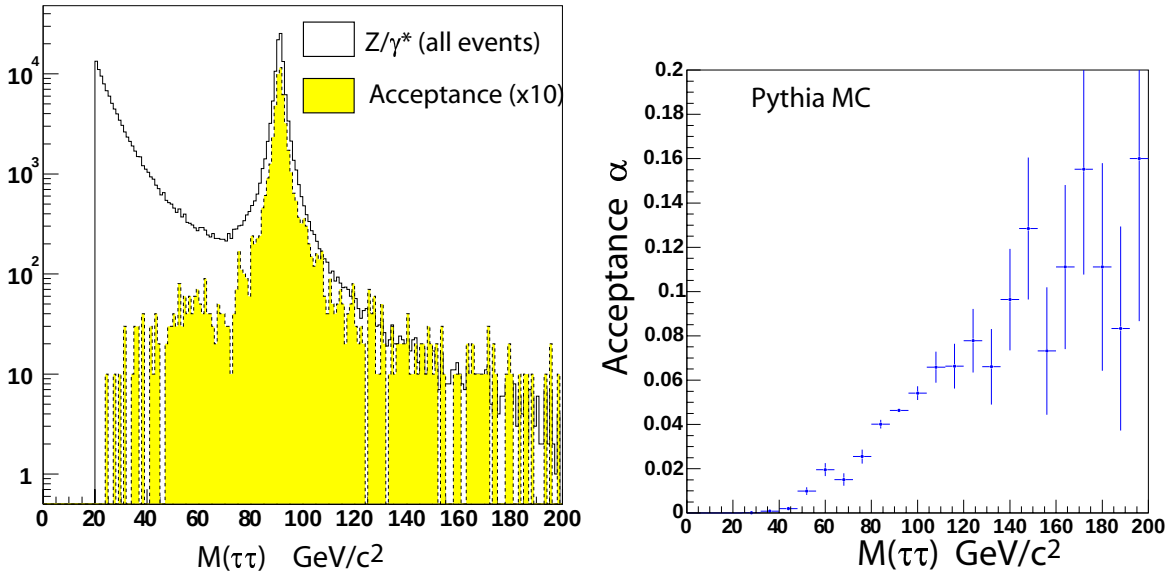

Figure 1: a): Distribution of $M_{\tau\tau}$ for Pythia $Z^0/\gamma^* \to \tau_e\tau_h$ process for all generated events (solid line) and events passing acceptance requirements (dashed line). b): Differential acceptance as a function of generated di-tau mass. Integrated acceptance for events in the mass window range $66 < M_{\tau\tau} < 116\,\mathrm{GeV}/c^2$ is $\alpha_0 = 0.0455 \pm 0.0006$.

Correction for $Z/\gamma* \to \tau\tau$ Outside the Window

Figure 1a shows the distribution of $M_{\tau\tau}$ for all generated events (solid) and for events passing acceptance requirements (dashed line). Figure 1b shows their ratio. We calculate the average acceptance to be $\alpha_0 = 0.0455 \pm 0.0006$ and will treat the contribution of events from outside the mass window as a correction (additional signal contribution) to the cross-section measurement.

We use MC to estimate the fraction of events originating outside the mass window that would pass acceptance requirement, and the correction is $f^{\alpha}_{\gamma*} = 1.055 \pm 0.004(stat) \pm 0.002(syst)$ calculated as the ratio of all events passing acceptance cuts with the generator di-tau mass, $M_{\tau\tau} > 20$ GeV, to the number of events passing acceptance cuts and with the true di-tau invariant mass inside the mass window. Of these events, roughly half comes from higher invariant masses than the window we use, while the other half is coming from lower invariant masses. The systematical uncertainty quoted for $f^{\alpha}_{\gamma*}$ is estimated by varying CTEQ6 PDFs. We estimate that the uncertinty on the number of events outside the window (which constitute about 5% of all events) is roughly 4%. As a result, we obtain a total uncertainty of 0.2% relative to the full signal acceptance.

Efficiency of $|\Delta z| < 60$ cm Cut

We correct acceptance for known small difference between data and MC in the efficiency of $|z_0^{e-trk}| < 60$ cm. For the $|z_0^{e-trk}| < 60$ cm cut, the MC predicts $\varepsilon_{MC}^{|z_0|<60\,cm} = 0.947 \pm 0.005$, while the efficiency measured in data is $\varepsilon_{DATA}^{|z_0|<60\,cm} = 0.950 \pm 0.002(stat) \pm 0.003(syst)$. This results in a scale factor of $f^{|z_0|<60\,cm} = 1.003 \pm 0.003$.

Track Reconstruction Efficiency

Based on the studies of track reconstruction efficiency in W events [18], which revealed no difference between data and MC within the accuracy of the measurement, we assign a systematic uncertainty of 0.4% per track [18] due to understanding of tracking reconstruction efficiency for electron track and for the seed track in 1-prong taus, which are expected to be similar. Case of 3-prong taus is somewhat different because presence of additional tracks creates higher occupancies that may have larger effect on pattern recognition.

To assign a conservative systematic uncertainty, we use results obtained in the measurement of the $D^{\pm}$[3] meson production rate [5]. In [5], track reconstruction efficiencies were measured by embedding $D^{\pm}$ mesons in real data events and varying appropriate resolutions (hit widths etc.). Measurement was performed for several ranges of the transverse momentum of $D^{\pm}$ (including range of $p_T > 20$ GeV/$c$relevant to this analysis). We assign the quoted in [5] uncertainty of 3% as a systematic error in the knowledge of track reconstruction efficiency for events with a 3-prong tau. Note that 3-prong taus constitute about 1/3 of 1 and 3-prong taus, and thus the average systematic uncertainty needs to be weighted accordingly:

$$\varepsilon = f_{1-pr} \times (\varepsilon_e + \varepsilon_{1-pr\,\tau}) + f_{3-pr} \times \sqrt{(\varepsilon_e^2 + \varepsilon_{3-pr\,\tau}^2)} \quad (5)$$

The average weighted uncertainty is 1.4% per event.

Cut on the Number of Towers in a Tau Cluster

We also studied the effect of a cut in reconstruction on the maximum number of towers in tau cluster, which is set to 6 towers. In fact, there is a difference between data and MC that is yet again related to the defficiencies in the simulation of the lateral profile of a hadronic shower in the calorimeter. Showers are wider in data than in MC, which result in a larger average number of towers in a tau candidate. However, because this cuts is extremely loose (it has nearly hundred percent efficiency), at the end the difference between data and MC is tiny. We discuss this issue in the tau ID section and refer to [13] for details.

Neutral Pion Reconstruction

Another possible systematic effect can be due to differences between data and MC for the rate of π^0 losses. For example, a π^0 is vetoed if there is a nearby track and different shape and size of showermax clusters in data and MC could in principle make this rate difference non-negligible leading to differences in the reconstructed energy spectra and different efficiency of passing threshold $E_T > 15$ GeVcut. Tau energy correction [7] is expected to compensate for these possible differences. This correction is designed to catch cases when π^0 is lost (e.g. a significant EM deposition in excess of what one expects from reconstructed tracks would indicate a lost π^0). To verify that the effect on acceptance is negligible, we used MC events in which we randomly "lost" a fraction of reconstructed π^0's and found that the change in acceptance is small, e.g. in an extreme case when all π^0's were "lost", acceptance has changed by about 1%.

Calorimeter Energy Scale and Resolution

We completely ignore uncertainties associated with the EM calorimeter energy scale and resolution, as those were found to be completely negligible in the previous version of this analysis[1]. The hadronic

[3]Note that $D^{\pm}$ mesons are very similar to the 3-prong taus making such comparisons valid.

Uncorrected Acceptance	$\alpha_0 = 0.0462 \pm 0.0002$	
Effect	Scale Factor	Syst. Uncertainty [%]
Track Reconstruction		1.4
$\lvert z_0 \rvert < 60$ cm	$f^{\lvert z_0 \rvert < 60\ cm} = 1.003$	
Mass Window Cut	$f^{\alpha}_{\gamma^*} = 1.055$	0.3
Material Uncertainty		1.3
PDF		2.2
Total:	1.058	2.9
Corrected Acceptance	$\alpha = 0.0489 \pm 0.0002(stat) \pm 0.0014(syst)$	

Table 4: Acceptance Scale Factors and Uncertainties. Note that all uncertainties quoted are relative to the acceptance.

calorimeter energy scale affects the tau reconstruction that requires the seed tower of the tau candidate to pass $E_T > 5$ GeV threshold. Taus, on average, have their energy split roughly equally between hadronic and EM calorimeters, so we estimate the uncertainty in the acceptance by varying the threshold of the seed tower up and down by 3%, and the resultant change is 0.2%. This is much smaller than other uncertainties and we choose to ignore it. Effects related to the knowledge of track p_T resolution we previously found to be negligible[1] and we ignore them as well.

For material uncertainty, we assign a systematic uncertainty of 1.3%, which is the same value as in [4] and is an upper limit for our case (note that the number in [4] accounts for two electron legs and also the material description in MC has greatly improved since). As a cross-check, we compared acceptance obtained with 5.3.3 MC and an older 4.9.1hpt3 sample[4] and find that the numbers are in statistical agreement (statistical uncertainty was at the level of 2%).

Systematic Uncertainties due to Parton Distribution Functions

We use a standard method used by the Z/W Cross-Section Group [8] to estimate the uncertainty as a function of Z rapidity. Figure 2a shows the distribution of Z-boson rapidity, η_Z, for all generated $Z \to \tau\tau$ events (solid line) and for events passing acceptance requirements (dashed line). Their ratio (differential acceptance) is shown in Figure 2b. This information is used to calculate the PDF uncertainties using CTEQ6 PDF "eigenvectors". We separately sum up in quadrature positive and negative corrections to the acceptance for each of the 20 eigenvectors. If both "positive" and "negative" shifts for any of the PDF eigenvectors happen to result in a positive (or negative) change in the acceptance, we use the one resulting in the larger change as positive (negative) uncertainty and the negative (positive) uncertainty is set to zero for this particular eigenvector. Final calculation predicts about 2.2% systematic uncertainty on the geometrical and kinematical acceptance.

5.2 Summary of Scale Fators and Uncertainties for Acceptance

Table 4 shows all the scale factors and associated uncertainties combined.

[4]This sample had a large underestimation of the amount of material, thus any comparisons should be considered as extremely conservative.

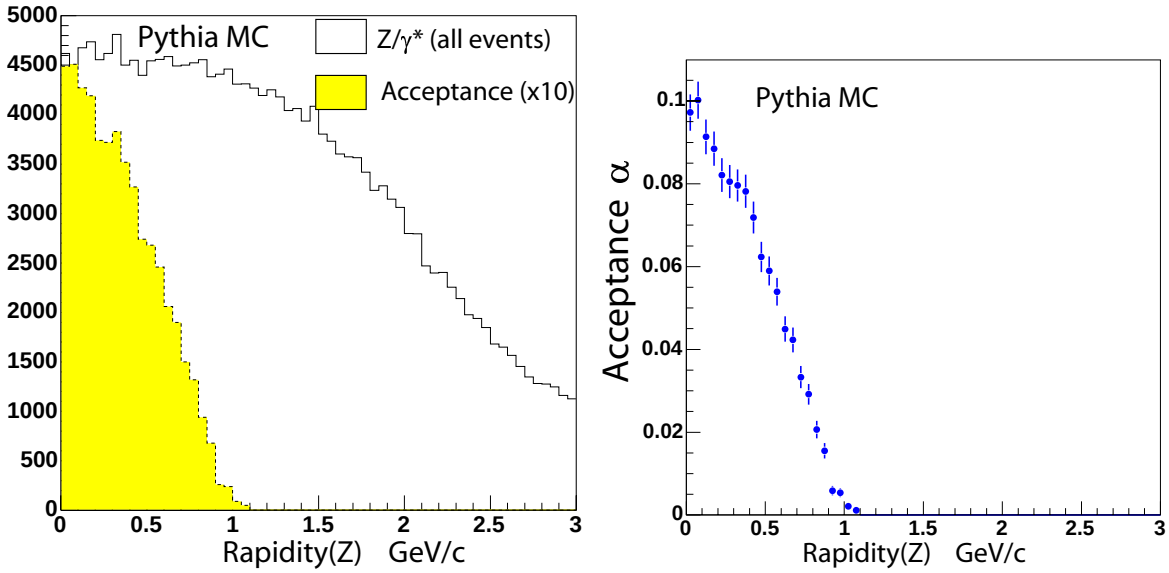

Figure 2: a) Distribution of Z-boson rapidity, η_Z, for all generated $Z \to \tau\tau$ events (solid line) and for events passing acceptance requirements (lower histogram, scaled by 5 for better visualization); b) differential acceptance as a function of η_Z.

6 Efficiencies

6.1 Electron Identification cuts

We estimate the efficency of the electron identification cuts using MC events passing the acceptance cuts and scale the efficiency using scale factors from [4]. We do not require the presence of the primary vertex, so for the track impact parameter cut we use the beam (x,y) position. Then the efficency of the isolation cut that is unique to this analysis is calculated using MC and compared with data for the $Z \to ee$ events where we apply the same cut. In the previous version of MC (4.9.1 series) we found a difference of about 4% between data and MC[13], which was related to a wrong rate of conversions due to lack of material in simulation. In the new MC there is no apparent disagreement, e.g. see [14], and we assign a systematic error of 1.5% on the track isolation cut efficiency and 1.0% on the π^0 isolation. For other cuts, we use an overall scale factor 1.000 ± 0.005 obtained in [18] for standard electron ID cuts excluding isolations. Dependence of the efficiency on electron energy is mostly governed by the amount of material, which is known to be accurate in current MC, and therefore should be reliably predicted. As a cross-check, in [10] we have measured the scale factor for events with electron $E_T \geq 6$ GeVusing upsilon events and found that the scale factor is consistent with 1.0 within the statistics (typical statistical uncertainty was of the order of 2%).

6.2 Tau Identification Cuts

There is a detailed description of the tau reconstruction and definitions of cut variables in CDF note 6552; we refer readers there. Compared to that version of this analysis, we since have developed a better

Cut	MC Efficiency [%]	Systematic Uncertainty [%]
Track Quality $3\times2\times5$(hits)	99.94 ± 0.01	
$E^{had}/E^{em} < 0.055 + 0.00045\times E$	98.02 ± 0.07	
$E/P < 2$ or $E > 100$ GeV	96.44 ± 0.09	
$-3 < Q_e\Delta X_{CES} < 1.5$ cm	99.02 ± 0.05	
$\lvert\Delta Z_{CES}\rvert < 3$ cm	99.72 ± 0.03	
CES $\chi^2\lvert_z < 10$	96.62 ± 0.09	
$L_{shr} < 0.2$	98.53 ± 0.06	
$\lvert d_0\rvert < 0.2$ cm	99.21 ± 0.04	
Correction[18]		0.5
$I_{trk}^{\Delta R<0.4} \leq 1$ GeV/c	82.85 ± 0.19	1.5
$I_{\pi^0}^{0.22<\Delta R<0.4} \leq 0.2$ GeV/c	97.29 ± 0.09	1.0
Cumulative	71.0 ± 0.2	1.9
Efficiency used	$71.0\pm0.2(stat)\pm1.3(syst)$	

Table 5: Efficiency of electron ID cuts. We use MC efficiency as a default with the exception of the ΔZ_{CES} cut, which is known to have problems in the MC version used. Efficiency of the ΔZ_{CES} cut is corrected to be consistent with a measurement using $Z \to ee$ showing full efficiency. Overall correction factor for electron ID efficiencies excluding isolations was obtained in [18]. Systematic uncertainties quoted are defined relative to the cumulative efficiency.

optimized tau energy correction[5]. Also, due to known problems of the current dataset, we used a fixed cone of 10^0 for the π^0 isolation definition.

Previously [2], we found that certain tau cuts are not well described by MC with the discrepancy especially pronounced for lower p_T taus. The cuts in question are related to the modelling of the (hadronic) showering in the calorimeter and special features of the calorimeter clustering used in tau reconstruction. Examples of such cuts are calorimeter isolation and lateral profile of the tau shower. Data suggest that showers are on average wider than predicted by Monte Carlo (this problem is likely related to not fully adequate showering parametrization in QFL/GFLASH and is in agreement with the observed discrepancies between data and MC in Run I for the calorimeter based jet shape measurements). For this reason, we do not use cuts on tau calorimeter isolation.

In [13], we measured isolation efficiencies directly from the data using $Z \to ee$ and $W \to e\nu$ data. It was also compared to $W \to \tau\nu$ data and found to be in agreement, however we would like to point out that while $W \to \tau\nu$ sample is the largest source of real taus, there is an issue with limited control of the background making this naively "best" sample not really useful. Following the same method, we find no disagreement between data and 5.3.3 MC predictions, e.g. see [14].

Of the remaining cuts, the ξ-cut was tested using a sample of charged pions [13] collected on the same trigger as the ones used in this analysis. A set of tight cuts aiming at electron removal was applied to separate real charged pions. The distribution of ξ variable for selected tracks was compared to the MC expectation and within statistics (at the level of 2%) the two were in agreement. While this

[5]Main change is that tau candidates with a detected likely π^0 loss and that have high fraction of the energy deposited in EM (> 0.85) calorimeter are assigned the calorimeter measured cluster energy. This change has almost no effect on real taus, but is useful for backgrounds as it does not promote electrons faking taus to high energies.

2% uncertainty, strictly speaking, is directly applicable to 1-prong taus only, the case of 3-prong taus is expected to have even smaller uncertainty because of higher efficiency of the cut (while fractional uncertainty on the inefficiency, which is about 10% for 1-prong taus, is approximately constant, the inefficiency itself becomes smaller and therefore the remaining absolute systematic error gets smaller). Mathematically, one can show that the probability of a N-prong tau candidate to fail the $\xi < \xi_0$-cut is:

$$P(\xi < \xi_0) \sim \prod_{i=1}^{i=N} \int_{p_i=1}^{p_i=\infty} dp_i \times F(p_1, p_2, ..., p_N) \times \int_{E_i=0}^{E_i < \xi_0 \sum_{i=1}^{N} p_i - \sum_{k=i+1}^{N} E_k} f(E_i, p_i) dE_i, \quad (6)$$

where $F(p_1, p_2, ..., p_N)$ is the distribution of track momenta in an N-prong tau, and $f(E, p)$ is the distribution for the hadronic energy deposition, E of a track with momentum p. While the formula itself is complicated, one can easily spot a couple of important features by considering two extreme cases: (i) $p_1 >> p_2, p_3$ and (ii) $p_1 \simeq p_2 \sim p_3$ (relative weight of these cases is determined by $F(p_1, p_2, ..., p_N)$). In the first case, the integral is dominated by the part related to p_1 while the part related to p_2 and p_3 integrates into $\simeq 1$, which physically corresponds to small contribution of two soft tracks both into the energy deposition and into the momentum sum. Second case is very different because all tracks can contribute into energy deposition about equally, but as long as ξ_0 is small, most of the contribution comes from the regions where all $E_i/p_i \leq \xi_0$ making an effective product of inefficiencies. Back of an envelope calculation for a 3-prong case, taking the inefficiency for 1-prong case to be 0.10 ± 0.02 would be $\simeq (0.10 \pm 0.02)^3 \simeq 0.0010 \pm 0.0017$ leading to an uncertainty of a fraction of a percent. Important conclusion is that additional tracks "smear" the effect, and the uncertainty in inefficiency for a multi-prong tau is always bound by the 1-prong case. Therefore, for simplicity we keep the 2% uncertainty and consider it as a conservative estimate. Additional checks were made by us in the past by varying the value of ξ_0 cut, which changes the amount of $Z \to ee$ and $Z \to \tau\tau$ in opposite directions, and found that the cross-section estimate remained stable with respect to such variations showing that MC properly simulates effects related to the ξ efficiency.

Tau invariant mass cuts (tracks and tracks plus π^0's) are intentionally set to be nearly 100% efficient even though we believe that tighter mass cut choices are also accurately described ($m_\tau \geq 1.8$ GeV/c^2), e.g. see comparisons for very clean $W \to \tau\nu$ data and MC in [13, 14].

For the cut on the number of prongs in a tau candidate, the main factor is accurate simulation of the probability of finding a track from the UE in the tau cone (we call it "migration" effect). We have studied the track density flow around electrons in $Z \to ee$ events and, by varying the density of the tracks in MC, obtain the best match with data[6], we have found that the uncertainty is within 0.5%. This approach was re-used in [14] with the same result. The full list of cuts and corresponding efficiencies can be found in Table 6. Additional information on the determination of the systematic uncertainties is compiled in the Appendix to this note.

In the past, we also applied a correction for the requirement on the number of towers in a tau candidate. This requirement should logically be applied at the acceptance corrections level, but we keep it here to preserve consistency with [13]. Given that the scale factor was consistent with one, we now simply quote a systematic uncertainty and do not apply a special corection for it. The size of the effect was estimated by "widening" tau clusters and forcing agreement between data and MC $W \to \tau\nu$ samples, and the net effect was found to be very small. This is because the $N_{tow} < 6$ is a very loose cut and even drastic changes in the shape of the N_{tow} distribution do not affect the size of the far tail. We assign a

[6] MC adjustment was performed by selecting events with higher or smaller average number of extra min-bias interactions.

Cut	MC Efficiency [%]	Systematic Uncertainty [%]
Seed Track Quality $3 \times 2 \times 5$(hits)	99.71 ± 0.03	
$\lvert z_0^{\tau-seed} - z_0^{e-trk} \rvert \leq 5$ cm	99.45 ± 0.04	
$d_0^{\tau-seed} < 0.2$ cm	97.65 ± 0.09	
$\xi > 0.1$	93.23 ± 0.15	2.0
$M^{track} \leq 1.8$ GeV & $M^{track+\pi^0} \leq 2.5$ GeV	98.79 ± 0.05	0.4
$N_{trk}^{\tau,\,\Delta\Theta} = 0$ & $N_{trk}^{\tau,\,\Delta R} = 0$	81.42 ± 0.23	1.5
$I_{\pi^0}^{\tau,\,\Delta\Theta} \leq 0.6\,\mathrm{GeV}/c$	95.26 ± 0.14	0.5
$N_{trk}^{\tau\ cone}$ =1 or 3	87.41 ± 0.23	0.5
N_{tow} Correction		0.5
Cumulative	60.47 ± 0.28	3.0
Final Efficiency	$60.47 \pm 0.28(stat) \pm 1.8(syst)$	

Table 6: Efficiency of tau ID cuts. We quote MC predictions based on $Z \to \tau\tau$ analysis and quote corresponding scale factors. Systematic uncertainties quoted are defined relative to the cumulative efficiency.

Trigger	Average Efficiency [%]
$\varepsilon_{L1}^{e} \times \varepsilon_{L2}^{e} \times \varepsilon_{L3}^{e}$	$96.5 \pm 0.1 \pm 2.0$
$\varepsilon_{L1}^{\tau} \times \varepsilon_{L2}^{\tau} \times \varepsilon_{L3}^{\tau}$	$96.1 \pm 0.2 \pm 2.0$

Table 7: Average trigger efficiency.

systematic uncertainty of 0.5% obtained by varying the degree of shower "widening" in a range consistent with data. More details can be found in [13].

6.3 Trigger Efficiency

Trigger efficiencies for the lepton+track triggers were measured for each of the two legs separately using data taken over the same running period as the one used in this measurement.

We used a photon conversion sample to measure the efficiency for the electron leg as a function of electron E_T and associated track p_T, see [11, 12]. The average plateau efficiency for the electron leg is found to be approximately 97 percent.

For the track leg, the measurement of the trigger efficiency [15, 16] is made assuming that this leg is a hadronic tau, and the efficiency is parametrized as a function of several tau variables. In the course of measuring efficiencies, we verified that the trigger efficiencies for the two legs are independent, e.g. we compared the efficiency for events with a single tau candidate and for events with tau candidate and an additional loose lepton. The average efficiency for the track leg above 10 GeV/c is approximately 97 percent, and it shows continuous growth towards higher p_T. We attribute this tendency to a feature [15] of the XFT track finding algorithm.

We calculate the average trigger efficiency by convoluting the Pythia MC with the parametrized trigger efficiency functions. Table 7 is a summary of the trigger efficiencies for electron and tau legs in Z events.

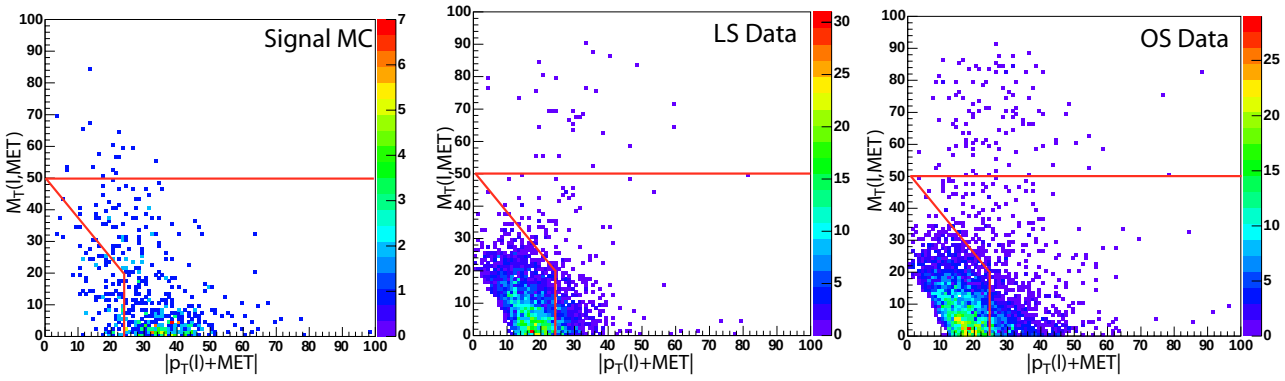

Figure 3: Distribution of M_T vs p_T for: a) signal $Z \to \tau\tau$ events obtained using Pythia and scaled to $\sigma(p\bar{p} \to Z) = 260$ pb^{-1}; b) LS data after all cuts except π^0 isolation dominated by backgrounds; c) OS data after all cuts except π^0 (includes signal and backgrounds).

6.4 Event Topolgy Cuts

To suppress W+jet and QCD backgrounds, we define two additional variables. The first one is the transverse mass of the electron and the missing transverse energy, M_T, defined as

$$M_T(e,\not\!\!E_T) = \sqrt{2 \times p_T^e \not\!\!E_T \times (1 - \cos\Delta\Theta)}\,, \tag{7}$$

where $\Delta\Theta$ is the 2D angle in the $r-\phi$ plane between the electron track and the missing E_T direction, and the second one is on the transverse momentum of the electron and the missing energy:

$$p_T(e,\not\!\!E_T) \equiv |\vec{p}_T^{\,e} + \vec{\not\!\!E}_T| \tag{8}$$

Corrections to Missing Transverse Energy Calculation

Missing transverse energy is corrected for overall energy scale, tower-by-tower corrections and the z_0 position of the electron candidate, all of which are standard. Additionally, we apply corrections for jets using Level 5 corrections (only if $E_T^{raw} > 10$ GeVand $E_T^{cor} > 15$) and taus to reflect lower E/P for charged hadrons and a correction for electron energy mismeasurement near the borders of the towers:

$$\vec{\not\!\!E}_T^{\,cor} = \vec{\not\!\!E}_T - (\vec{p}_T^{\,cor} - \vec{p}_T^{\,raw}) \tag{9}$$

In the case of jets, "raw" refers to the uncorrected jet energy; for correction we use standard Level 5 corrections. Similarly, for taus "raw" refers to the calorimeter energy of the tau cluster[7], while corrected energy is measured using tracks and π^0's with appropriate corrections.

[7]In addition to towers assigned to the tau cluster that are required to have $E_T > 1$ GeV, we add all adjacent towers to compensate for the inadequecies in the lateral shower profile simulation as discussed further in the note.

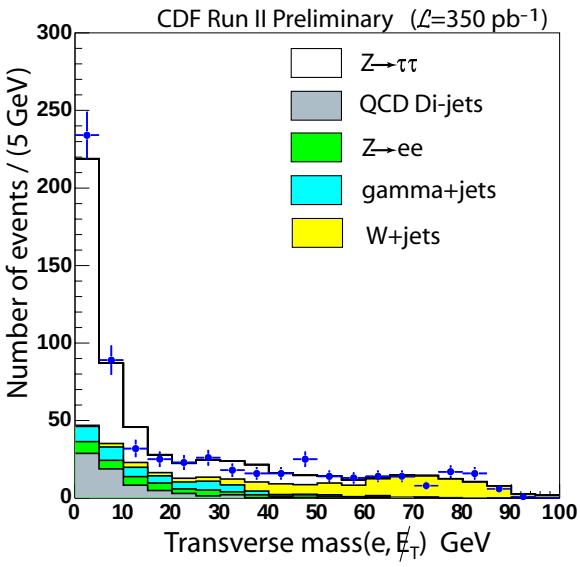

Figure 4: Distribution of transverse mass, M_T, for signal and backgrounds. $Z \to \tau\tau$ expectation (empty histogram) is obtained using Pythia MC and scaled to $\sigma(p\bar{p} \to Z) = 258$ pb^{-1}; $Z \to ee$ and W+jets are also using Pythia and expected NLO cross-sections. Prediction for QCD jets and γ+jets is obtained using data as described later in the note. Optimized value of M_T is found to be at 50 GeV/c^2.

Optimization

To show the discriminating power of the proposed cuts, in Figure 3a we present a distribution of M_T vs p_T for signal $Z \to \tau\tau$ events after applying acceptance requirements and identification requirements for electron and tau candidates. The distribution is obtained using Pythia MC and normalized to the luminosity in the data. Fig. 3b shows similar distribution for the LS data dominated by backgrounds.

The optimal choice of cuts is shown in Fig. 3. Optimization is performed using an iterative procedure for maximizing the significance, $S/\sqrt{S+B}$ (and also $S/\sqrt{S+2B}$ that implies that the systematic uncertainty in the background estimation is driven by the statistical uncertainty). In the process of optimization, we vary the level of the horizontal bar and the position of the break point, i.e. there are three parameters to optimize.

First, we maximize the significance using the final LS events as a background model. That would include most of the backgrounds, but will only partially include W+jets background that has an intrinsic charge asymmetry (larger fraction of OS events). We start with an arbitrary upper cut value for M_T (left corner point), and vary position of the break-point in 2D for maximum significance. After the initial point is obtained, we go to a one dimensional plot of the transverse mass, see Fig. 4, and find the optimal cut on M_T given the fixed position of the break-point. Then we fix the left corner point to the obtained M_T value and we repeat the first step for finding the optimal position of the break-point, and iterate again until convergence is achieved. The results are shown in Table 8.

Efficiency and Systematic Uncertainties

The efficiency of conversion removal and OS requirement for the signal is estimated using MC events. The systematic uncertainty is conservatively set to be equal to the deviation of the efficiency from unity[8]. The results are in Table 8. The efficiency of $Z \to ee$ removal for the signal is also estimated using MC events[9]. The results are in Table 8.

The efficiency of the topology cuts is estimated using MC. We varied the effect of corrections to $\not\!\!E_T$, namely for jets, taus and electrons. Effects related to jet corrections were found to be small, as expected, as the events in question rarely have any jets at all, and their contribution to the correction is small. Similarly, we turned on and off the correction for electron, both in data and in MC, and the change was also small, indicating that these effects are properly simulated.

Accurate estimation of the size of the effect on $\not\!\!E_T$ due to the tau correction is more complicated. In the default case we correct $\not\!\!E_T$ for the difference between the tau p_T measurement based on tracks and π^0's (which is the most accurate measurement of this quantity available), and the calorimeter measured tau cluster energy plus all adjacent towers. This last addition is important because taus in data have a wider shower profile, leading to differences beween data and MC in the amount of unclustered energy (data has more energy leaking into neighbouring towers). If one would simply use tau cluster energy, there will be an average effect of "turning" $\not\!\!E_T$ in the direction opposite to tau (thus, most of time in the direction of the electron) more often in data than in MC, which in turn leads to higher efficiency for passing event topology cuts in data events than in MC simulation. The reason for it is the long standing problem with the MC predicting a more narrow lateral profile for taus than indicated by the checks in data. This problem is traced to the simulation of the showers in the hadronic part of the calorimeter.

To estimate the size of this effect, we compare the default case to the case when the "raw" tau energy is calculated using only towers assigned to the tau cluster. That defines the "deviated" correction, which we apply both to data and MC, and repeat the full calculation of the cross section (including full background re-calculation) with the varied correction. We obtain a 2.4% difference in the value of the measured cross-section with the statistical uncertainty of each of the measurements at the level of 8%. Because there is a large correlation between the two samples, we choose to assign the 2.4% as an estimate of the systematic uncertainty on the efficiency of the event topology cuts due to $\not\!\!E_T$ measurement.

7 Backgrounds

On top of the signal $Z \to \tau\tau$ events, the selected sample has several background contributions. In the following, we describe these backgrounds and the methods we use to estimate their contribution starting with simple ones estimated using MC events, and following onto more difficult ones.

$Z/\gamma^* \to ee$ background events enter the sample if two requirements are satisfied: first, one of the electrons has to pass the anti-electron ξ tau cut (usually via strong Brem) and, second, the measured invariant mass of the two electron candidates has to fall outside the Z window mass cut.

W+jet background finds its way into our sample via a jet faking a tau candidate. This background is strongly suppressed by the event topology cuts that effectively require remaining W+jet events to have

[8] We also performed comparisons between conversion tagging rate in data and MC using $Z \to ee$ events that have shown no disagreement within statistical uncertainties ($\simeq 0.2 - 0.3\%$).

[9] Events removed by the Z-veto were studied and we confirm that vast majority of them is very consistent with the expectation that these are $Z \to ee$ with one of the legs undergoing strong brem making it pass the anti-electron ξ-cut

Cut	MC Efficiency [%]	Syst.ematic Uncertainty [%])
$Q_e \times Q_\tau = -1$	99.27 ± 0.06	0.8
Conversion Removal	99.10 ± 0.07	0.8
Z Removal	97.33 ± 0.12	1.0
$p_T > 24$ or $M_T > 50 - 1.25 \times p_T$	81.9 ± 0.3	2.4
$M_T(e, \not\!\!E_T) < 50$ GeV	96.9 ± 0.2	(incl. above)
Cumulative	76.0 ± 0.3	2.8
Efficiency used	$76.0 \pm 0.3(stat) \pm 2.1(syst)$	

Table 8: Efficiency of event level cuts. MC prediction is chosen as default. Systematic uncertainties quoted are defined relative to the cumulative efficiency.

large transverse momentum of the W boson ($\simeq p_T(e, \not\!\!E_T)$) and low M_T thus deminishing this contribution. This is a simplification compared to the previous measurement, where low statistics did not allow careful comparison of W+jets in MC and data forcing us to use a complicated fitting scheme to disentangle this background.

$tt-bar$ and diboson backgrounds are small, literally a few events are expected, and we choose to discard them completely given the estimate that their effect on the cross-section measurement is at the level of 1-2%, which is much smaller than statistical or systematical uncertainties involved in the measurement.

Light-quark QCD backgrounds usually get into the sample via one jet faking an electron (e.g. conversions), while the other jet (or a part of it) is faking a τ candidate. Typically, track multiplicity for fake τ's from jets peaks in a two-prong bin for the range of jet E_T and p_T^τ characteristic for this analysis, e.g. see [17]. Heavy flavor QCD backgrounds have two important features that distinguish the way they penetrate the Z dataset. First, they have "real" electrons from the semileptonic decays of heavy flavor quarks, and, second, "tau" fakes from heavy flavor jets have a different shape of the multiplicity distribution. This difference is likely due to the decay modes of b mesons; e.g., some of the "heavy" mesons are ready candidates for fake τ's ($D^\pm$ has mass of $1.9\,\mathrm{GeV}/c^2$ compared to $m_\tau = 1.8\,\mathrm{GeV}/c^2$ and decays into three pions).

We found a sizeable background contribution from the $p\overline{p} \to \gamma$+jet production process. The main mechanism is via photon conversion while the jet is faking a τ. Taking into account that we explicitely remove conversion electrons and that most of the events have to pass the tight $p_T(e, \not\!\!E_T) > 24\,\mathrm{GeV}/c$ cut, these events typically have very assymmetric p_T's of the conversion electrons, relatively low $\not\!\!E_T$ and have one or more recoiling jets. These events, unlike QCD events, typically have a well isolated electron. The reason is that conversion removal selects events with no visible conversion partner track and, unlike dijets, there are not many other surrounding tracks to boost the I^e_{trk} value. In [17], we have shown that the γ+jet process is a dominant contribution to backgrounds with an isolated lepton. In this analysis, we have tighter cuts compared to [17] in order to suppress this background further, but it is still quite sizeable. An important feature of the γ+jet process is that it is *charge blind*, i.e. the number of events in OS data is statistically the same as in the LS data. Note that this background is specific to the $Z \to \tau_e \tau_h$ mode and is not present in $Z \to \tau_\mu \tau_h$.

7.1 $Z \to ee$, $t\bar{t}$ and Diboson Backgrounds

We use MC events to estimate the backgrounds due to $Z \to ee$, $t\bar{t}$ and diboson backgrounds. Apart from $Z \to ee$, the top/diboson backgrounds are relatively small, and we choose to discard them.

$Z/\gamma^* \to ee$ background events enter the sample via two modes: (i) one of the electrons passes the hadronic tau requirements by leaving substantial deposition in the hadronic portion of the calorimeter, or (ii) the recoil jet in $Z/\gamma^* \to ee$ is misidentified for a hadronic tau while the event passes the $Z \to ee$ candidate removal either because one of the electrons is not reconstructed (e.g. fall outside the detector coverage) or if the invariant mass of the two electron candidates falls outside the Z window mass cut. Main mechanism responsible for this is strong Bremstrahlung, making the electron track to be soft (this is how it passes ξ cut); if the Brem photon and track deposit energy in adjacent towers in ϕ, the electron energy is underestimated (this is a feature of electron clustering that does not combine adjacent towers in ϕ) leading to a lower reconstructed mass of the pair. The probability of an electron to be misidentified as a tau is expected to be well simulated in the MC, e.g. in [9] a measurement of the fake rates for $Z \to ee$ event to pass ξ cut of 0.1 was made and compared to MC and found to agree. In the previous analysis [1], we verified that the cross-section measurement remained stable with respect to varying the cut on ξ. We assign a systematic uncertainty of 20% on the size of the $Z \to ee$ background, which leads to about 2% uncertainty on the cross-section.

Note that with the procedure used in this measurement, we are not sensitive to whether the MC properly simulates the probability of a jet to be misidentified as a tau (second $Z \to ee$ mode in above), because any mismatch between data and MC is subtracted anyway as part of the QCD subtraction as described later on.

7.2 W+jets

In general, one does not expect a very good agreement between data and MC predictions for W+jets background. The level of agreement is determined by how well MC predicts the probability of a jet to fake a tau candidate, and relies on fine details of the jet fragmentation restricted to a relatively small fraction of the phase space. In the previous version of this measurement, low statistics did not allow a careful comparison of W+jets in MC and data forcing us to use a complicated fitting scheme to disentangle this background to avoid reliance on the MC. Now, with much larger statistics, we can compare data and MC predictions in the high M_T region to obtain the scaling factor, f^W for this background. As it will be shown later, $f^W \simeq 0.7 - 0.8$

7.3 QCD

An important feature common for QCD backgrounds is that if one plots tracking isolation, $I_{trk}^{e,\Delta R}$, defined in Section 4.2, to the first order the distribution is *flat* for fake electrons inside jets[10]. This allows estimation of the number of events in the signal region ($I_{trk}^{e,\Delta R} < 1$ GeV) by using events in the "sideband" region $2 < I_{trk}^{e,\Delta R} < 8$ GeV:

$$N_{A-I}^{QCD} = r \times N_{A-II},\ r = 1/6. \tag{10}$$

[10]We have checked this in MC samples of generic dijets and $b\bar{b}$ and while statistics is limited, they all are consistent with being flat

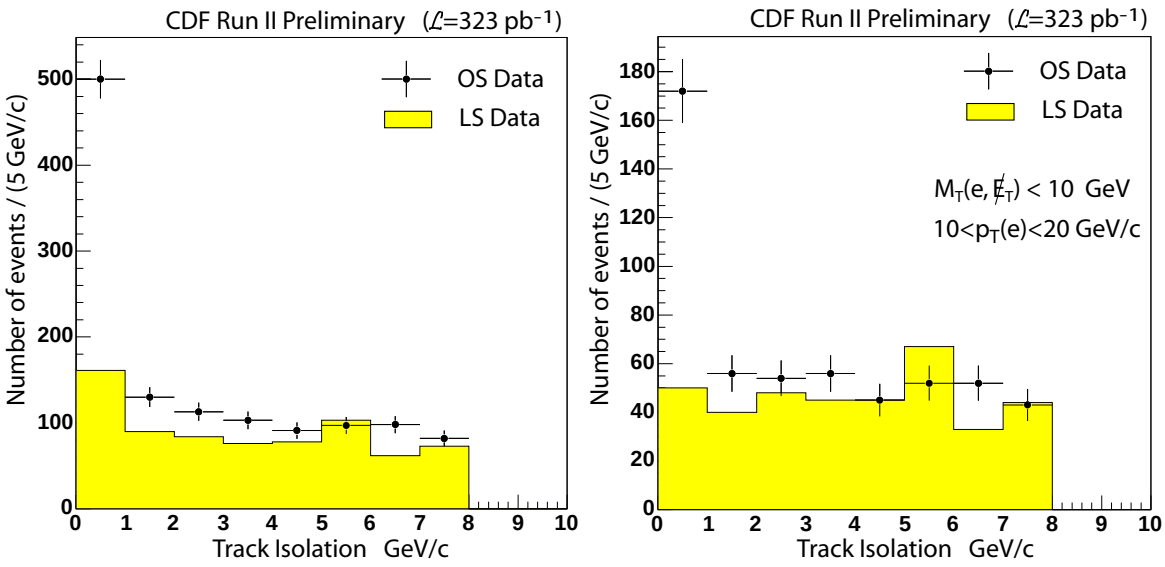

Figure 5: a) "N-1" distribution of the electron track isolation, $I_{trk}^{e-trk,\,\Delta R}$ for OS and LS $Z \to \tau\tau$ candidate events after all analysis cuts, b) Same distribution, but with additional cuts, $M_T < 10$ GeV$/c^2$, $10 < E_T^e < 20$ GeV that suppress W+jets and γ+jets contamination, LS events in this case are nearly pure sample of QCD jet events.

In [2], we have demonstrated that this technique works very well not only for event counting, but for a variety of reasonable distributions: measuring the shape of the distribution using events with non-isolated electrons and rescaling it according to Eq. 10 gives an accurate description of the background shape[11]. Figure 5a) shows the distribution of $I_{trk}^{e,\,\Delta R}$, the electron track isolation, for events with 1 and 3 prong tau candidates passing all other cuts. Although contamination of the γ+jets events in this sample is significant (excess in the isolated region), one can still note the flat shape of the isolation for LS events. Figure 5b) shows a similar distribution, but with additional kinematical cuts aimed to suppress γ+jets contamination ($M_T < 10$ GeV$/c^2$, $10 < E_T^e < 20$ GeV - the effectiveness of these cuts is evident by looking at kinematical distributions shown in the end of the note). We use these events to estimate the uncertainty in the "flatness" of QCD background from data and find $r = 0.17 \pm 0.02$.

7.4 γ+jet

As mentioned before, an important feature of γ+jet is that it is *charge blind*, i.e. number of events in OS data is statistically the same as in the LS data. Although this is fairly obvious, we verified OS/LS ratio in [17]. This feature allows estimating the number of γ+jets background events in the signal events (OS) by measuring the excess of the events with isolated electron over the flat (QCD) background in LS data, after subtracting contamination from W+jets, $Z \to ee$ and signal.

[11] Using events with very poorly isolated leptons may produce undesirable biases in kinematics of the event, therefore we limit the non-isolated region to $I_{trk} < 8$ GeV$/c$. We verified that this choice is safe by comparing predictions for backgrounds obtained from two sub-regions of $2 < I < 5$ and $5 < I < 8$ GeV$/c$.

Shape of the γ+jets background is estimated from the data using events with a converting γ+tau candidate sample. We start by requiring that an event has a good electron that is tagged as a part of a conversion pair. We then reconstruct photon momentum as a sum of the four-vectors of the two converting electrons. From this point on, we treat the photon as if it was a good electron and apply all analysis cuts. The total normalization, f^{γ}, then can be scaled to the excess of LS events in region A-I in LS events, as described above. Again, similar to the $Z \to ee$ and W+jets case, the overall measurement is not sensitive to predictions in the non-isolated regions, because any discrepancy is absorbed in the QCD estimation by construction.

7.5 Signal Extraction Method

To extract the number of signal and background events, we remove $M_T(e, \not\!\!E_T)$ and track isolation cuts and drop the OS charge requirement of electron and tau candidates. Then, for OS and LS events separately, we define four regions in the I^e_{trk} vs $M_T(e, \not\!\!E_T)$ plane, denoted as A-I/II, B-I/II, as defined in Table 9.

Table 9: Definition of the regions used in estimating the number of signal events. Note that by constuction region A-I is the signal region. These regions are defined separately for OS and LS data.

	A		B	
	I	II	I	II
M_T GeV/c^2	(0:50)		(50:100)	
$I^{\Delta R,\,e}_{trk}$ GeV/c	(0:1)	(2:8)	(0:1)	(2:8)
Dominant Contribution	$Z \to \tau\tau$	QCD	W+jet	QCD

With these definitions, signal events are expected to occupy region A-I while W+jet backgrounds dominate in region B-I. Note that this separation is not exact and each region has non-negligible contributions from more than one process. To take this into account, one can write for each of the regions the expected number of events as:

$$N_X = N_X^{Z\to\tau\tau} + N_X^{QCD} + N_X^{\gamma j} + N_X^{W j} + N_X^{Z\to ee}\,, \tag{11}$$

where X denotes the region A-I, A-II, B-I, B-II for OS or LS data.

In Tables 10 and 11 we show the observed number of events in each category and list background estimations. Parameters f for absolute scales of the signal and backgrounds are arbitrary, although we rescaled them so that $f \simeq 1$ (except for $f^W \simeq 0.73$) to enable readers make their own back-of-the-envelope calculations. For signal, $f \simeq 1$ roughly corresponds to signal cross-section of 260 pb.

The information in Tables 10 and 11 is sufficient to extract the number of expected signal events. One can fit the expected number of events to the observed one in all regions simultaneously and extract all the normalizations (and integrate over those we don't need). An equivalent, but simpler, method is as follows:

- Start with any f^s ($f^s \simeq 1$ will make convergence faster);
- Obtain the parameters f^W from the high M_T region, B-I, dominated by W+jets, using OS and LS (together, or separately);

Table 10: Number of OS events in each of the regions. Normalization parameters f are generally arbitrary, although $f^W = 1.0$ would correspond to default MC prediction for W+jets, and $f^s = 1$ roughly corresponds to the emasured $\sigma(p\bar{p} \to Z \to \tau\tau)$. Parameter r is expected to be $1/6$, which corresponds to an exact scaling of QCD jet events with track isolation (for reference, QCD contribution in region A-I is 68.6).

Process	A-I	A-II	B-I	B-II
$Z \to ee$	34.8 ± 1.4	3.2 ± 0.4	3.9 ± 0.5	0.28 ± 0.14
W+jets	$\frac{f^W}{0.73}(36.6 \pm 3.5)$	$\frac{f^W}{0.73}(2.0 \pm 1.0)$	$\frac{f^W}{0.73}(87.5 \pm 5.3)$	$\frac{f^W}{0.73}(7.0 \pm 1.9)$
γ+jets	$f^\gamma(47.8 \pm 2.2)$	$f^\gamma(29.9 \pm 1.9)$	$f^\gamma(1.4 \pm 0.4)$	$f^\gamma(0.10 \pm 0.10)$
QCD di-jets	$r \times Q^{OS}_{A-II}$	Q^{OS}_{A-II}	$r \times Q^{OS}_{B-II}$	Q^{OS}_{B-II}
$Z \to \tau\tau$	$f^s(316.4 \pm 7.9)$	$f^s(21.5 \pm 1.9)$	$f^s(10.3 \pm 1.4)$	$f^s(0.78 \pm 0.35)$
Data	504	468	105	12

Table 11: Number of LS events in each of the regions. Normalization parameters f are generally arbitrary, although $f^W = 1.0$ would correspond to default MC prediction for W+jets, and $f^s = 1$ roughly corresponds to $\sigma(p\bar{p} \to Z \to \tau\tau) \simeq 260$ pb. Parameter r is expected to be $1/6$, which would corresponds to an exact scaling of QCD jet events with track isolation. All uncertainties are statistical only.

Process	A-I	A-II	B-I	B-II
$Z \to ee$	3.9 ± 0.5	0.28 ± 0.13	0.51 ± 0.17	0.11 ± 0.08
W+jets	$\frac{f^W}{0.73}(15.4 \pm 2.3)$	$\frac{f^W}{0.73}(1.2 \pm 0.9)$	$\frac{f^W}{0.73}(27.8 \pm 3.0)$	$\frac{f^W}{0.73}(2.2 \pm 1.0)$
γ+jets	$f^\gamma(47.8 \pm 2.2)$	$f^\gamma(29.9 \pm 1.9)$	$f^\gamma(1.4 \pm 0.4)$	$f^\gamma(0.10 \pm 0.10)$
QCD di-jets	$r \times Q^{LS}_{A-II}$	Q^{LS}_{A-II}	$r \times Q^{LS}_{B-II}$	Q^{LS}_{B-II}
$Z \to \tau\tau$	$f^s(3.9 \pm 0.9)$	$f^s(0.6 \pm 0.2)$	$f^s(0.0 \pm 0.1)$	$f^s(0.2 \pm 0.2$
Data	130	386	33	2

- Use region A-I for LS events to extract f^γ;
- Calculate f^s by requiring the sum of prediction and background to agree with the observed number of events
- Iterate using the newly obtained value of f^s until the desired level of convergence (e.g. $\simeq 1\%$ that would exceed the expected uncertainty of the measurement)

At the point of convergence $f^W = 0.73 \pm 0.10$, $f^\gamma = 1.00 \pm 0.23$. Note that the numbers are completely uncorrelated because the estimates come from different regions in data, and the error is determined by varying the parameter until the statistical uncertainty on the background estimation in the region of interest changes by one sigma. The case of r is more tricky, because in this case QCD background and $\gamma+$ *jet* separately change quite significantly as varying r is equivalent to reassigning events from QCD category to γ+jets. Thus, in this case we calculate the uncertainty on the sum of QCD and γ+jets backgrounds and treat it as a separate uncertainty associated with the precision in the knowledge of r value.

As a cross-check, one may extract f^W from LS events only (in the iterative scheme, we use OS events to obtain this scaling factor), and the result is $f^W_{LS} = 0.82 \pm 0.15$, clearly indicating a good agreement with MC predictions for asymmetry.

To determine systematic uncertainty on the background estimation, we calculate the effect on the number of extracted signal events by varying the above parameters as follows:

- f^W within 0.73 ± 0.10 (separately from all others);
- Expected rate of $Z \to ee$ events by 20% (separately from all others);
- f^γ from 1.0 to 1.23 and 0.77 (separately from all others);
- r from $1/6$ to 0.15 and 0.18, (f^γ is re-calculated in each case, and the combined effect on the sum of QCD and γ+jets backgrounds is assigned as systematic uncertainty, and the variation in the sum is 3.0 events).

We then sum up all deviations in quadratures to obtain the systematic uncertainty associated with the background calculation, see Table 12 listing all backgrounds for region A, including statistical and systematical uncertainties.

Table 12: Number of observed events and background expectation for signal events. (*) Note that total systematic uncertainty includes an additional systematics associated with varying r from its default value of $1/6$ to 0.15 and 0.18, that resulted in additional systematic uncertainty of 3.0 events on the sum of backgrounds.

Process	Yield (in number of events)
$Z \to ee$	$34.8 \pm 1.4 \pm 7.0$
W+jets	$36.6 \pm 3.5 \pm 4.9$
γ+jets	$47.8 \pm 2.2 \pm 12.0$
QCD di-jets	68.6 ± 3.6
Total:	$187.7 \pm 5.7 \pm 15.0^*$
Data	504
$Z \to \tau\tau$	$316 \pm 23 \pm 15$

8 Cross-Section Calculation

With the definitions adopted earlier, we use the following formula for calculation of the cross-section:

$$\sigma(Z/\gamma^* \to \tau\tau) = \frac{1}{L}\frac{1}{2Br_{\tau\to e}Br_{\tau\to\tau_{had}}} \times \frac{N_{signal}}{\alpha\varepsilon^e_{ID}\varepsilon^e_{trig}\varepsilon^\tau_{ID}\varepsilon^\tau_{trig}\varepsilon_{event}} \tag{12}$$

where v^{signal} is measured rate of the signal events. PDG values for the branching ratios are $Br_{\tau\to e} = 17.84 \pm 0.06\%$ and $Br_{\tau\to\tau_{had}} = 64.79 \pm 0.08\%$.

Table 13: Tabulation of final systematic uncertainties.

	Systematic Uncertainty [%]
Signal events yield $N_{Z\to\tau\tau} = 316 \pm 23 \pm 15$	
Geometrical and kinematical acceptance (incl. PDFs)	3.0
Electron ID	1.9
Tau ID	3.0
Electron Trigger Efficiency	2.0
Tau Trigger Efficiency	2.0
Topology cuts	2.8
Background estimation	4.7
Total:	7.7
Cross-Section $\sigma(p\bar{p}\to Z)Br(Z\to\tau\tau) = 265 \pm 20(stat) \pm 21(syst) \pm 15(lumi)$ pb	

We outline all systematic uncertainties obtained earlier in Table 13. Note that PDF and energy uncertainties are absorbed into the acceptance uncertainty. Other uncertainties are negligible, e.g. there is a small effect due to ISR jets that can sometimes be reconstructed as hadronic taus: the size of the effect is estimated by dropping matching requirements between reconstructed and generated taus and is found to be very small (fraction of a percent). In addition, this effect is fully accounted in the background subtraction scheme where these events will be treated as charge symmetric backgrounds with an isolated electron (and fall into the γ+jet category).

The final result for the cross-section is $\sigma(p\bar{p}\to Z)Br(Z\to\tau\tau) = 265 \pm 20(stat) \pm 21(syst) \pm 15(lumi)$ pb. Table 13 collects all separate numbers contributing to the calculation.

9 Kinematical Distributions

We start with a plot of the invariant mass distribution of the $e-\tau-\not{E}_T$ system shown in Figure 6a. The data points correspond to the OS data, the histogram corresponds to the signal with measured cross-section plus backgrounds. Note that in the histogram for the expected signal, we allow events from outside the mass window cut (otherwise they should be considered as a background).

For γ+jet background, we use the shape of the distribution obtained from the conversion $\gamma+\tau$-candidate sample, while the normalization is set according to the number measured. For W+jet backgrounds, which has two components, $W\to\tau\nu\to e\nu\nu$ and $W\to e\nu$, we weight the two samples according to the luminosity of the MC samples and normalize the sum to the predicted number of W+jet events in the final sample. Similarly, we normalize the $Z\to ee$ background.

To demonstrate that the signal and backgrounds are well understood, in Figure 6b we plot the distribution for the track multiplicity of tau candidates with all backgrounds. The two-peaked structure characteristic of real taus is clearly present in the plot. The procedure for the background estimation is as follows: we drop requirements on the number of tracks in a tau candidate and the OS requirement. Backgrounds for QCD are measured directly and corrected by the same factors as for OS data case. The shape for the $\gamma+$ jet data is the one measured in data for the conversion $\gamma+\tau-$candidate data, EWK and W+jet background shapes are based on MC; normalization is obtained by forcing an agreement with the

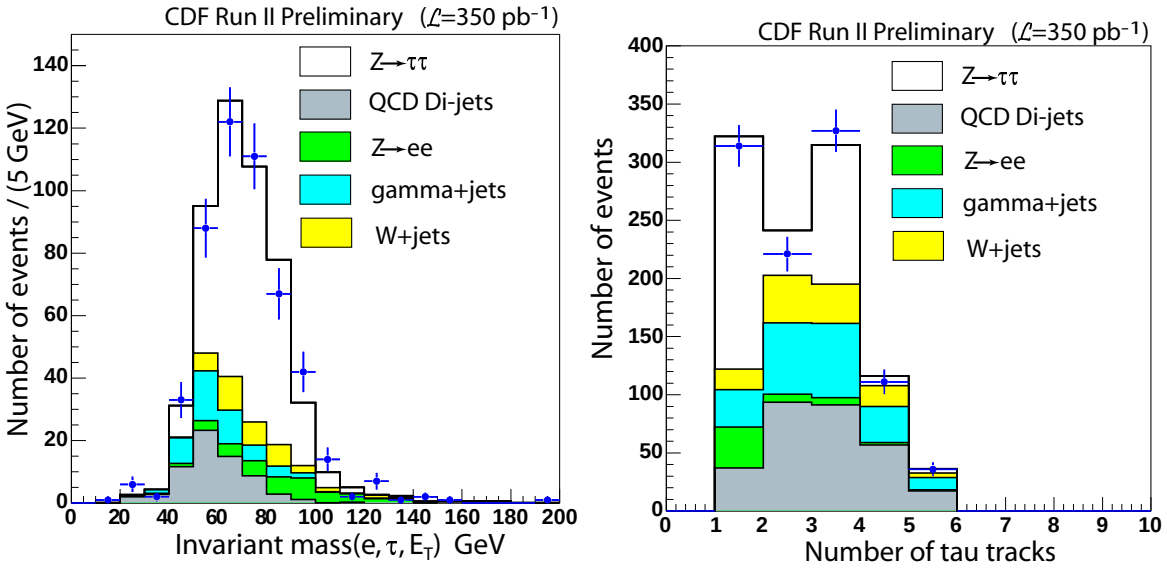

Figure 6: a) Distribution of the invariant mass of $e-\tau-\not\!\!E_T$ system for opposite sign events; b) prong multiplicity of τ candidates with the OS and $N_{trk}=1,3$ requirements dropped. In both plots data points correspond to the data, while the filled histograms to the expected signal and backgrounds placed on top of each other.

number of expected background contribution in the OS data sample.

For illustration purposes, in Figure 7 we plot the electron transverse energy, E_T^e, and the hadronic tau transverse momentum, p_T^τ, distributions with the same conventions.

For cross-checks, we select a "clean" sample of signal events by applying a tighter cut on the transverse mass of lepton and $\not\!\!E_T$, $M_T < 10$ GeV/c^2. Figure 8 shows the distribution of clean signal events as a function of variable $p_T = |\vec{p}_T^{\,e} + \vec{\not\!\!E}_T|$ used as an event topology cut, and the number of jets ($E_T > 15$ GeV).

A few additional plots were made to demonstrate good agreement between kinematical distributions in data and expectation. Figure 9a shows the $\Delta\phi(\tau_e, \tau_h)$ distribution for final events. Figure 9b shows "N-1" distribution for the π^0 isolation, I_{π^0}, in the final events validating the good understanding of isolation efficiencies.

Figure 10 shows the distribution of the invariant mass of electron-tau-$\not\!\!E_T$ system for 1-prong and 3-prong events separately, and finally Figure 11 shows the distribution of the $p_T = |\vec{p}_T^{\,e} + \vec{\not\!\!E}_T|$ variable, which is one of the event topology cuts. This plot serves as visual confirmation of the correctness of the optimization procedure and also confirms that this variable is well simulated by MC.

10 Summary

We have presented the first CDF measurement of the $p\bar{p} \to Z \to \tau\tau$ process cross-section in a channel with one tau decaying into an electron and the other one into hadrons. The measured value is $\sigma(p\bar{p} \to Z)Br(Z \to \tau\tau) = 265 \pm 20(stat) \pm 21(syst) \pm 15(lumi)$ pb and is in good agreement with the

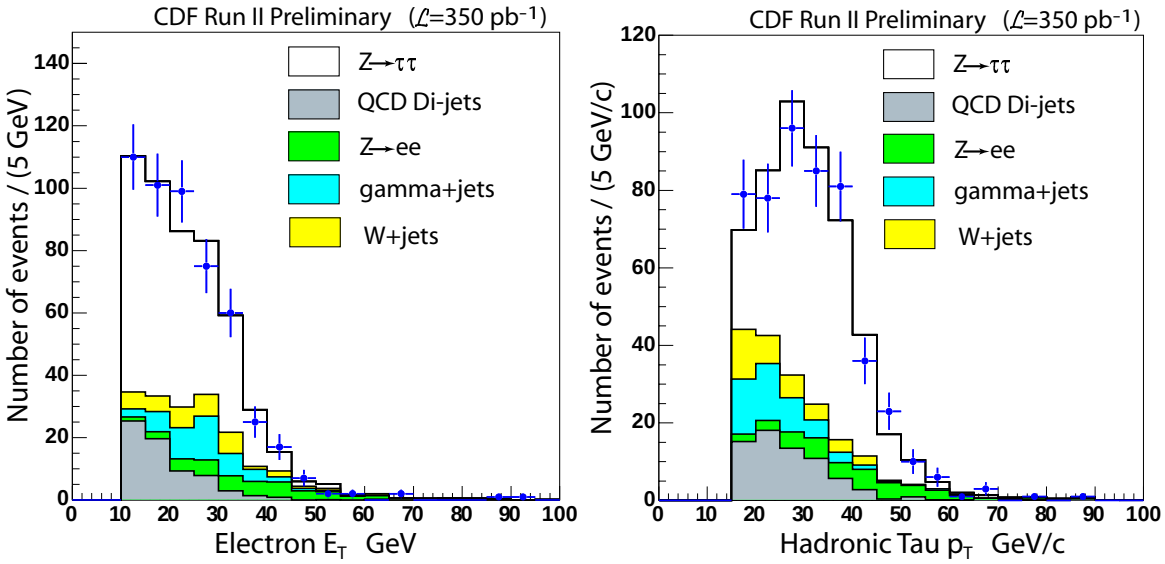

Figure 7: Distribution of: a) the electron E_T; b) τ candidate p_T for opposite-sign events passing all selection requirements.

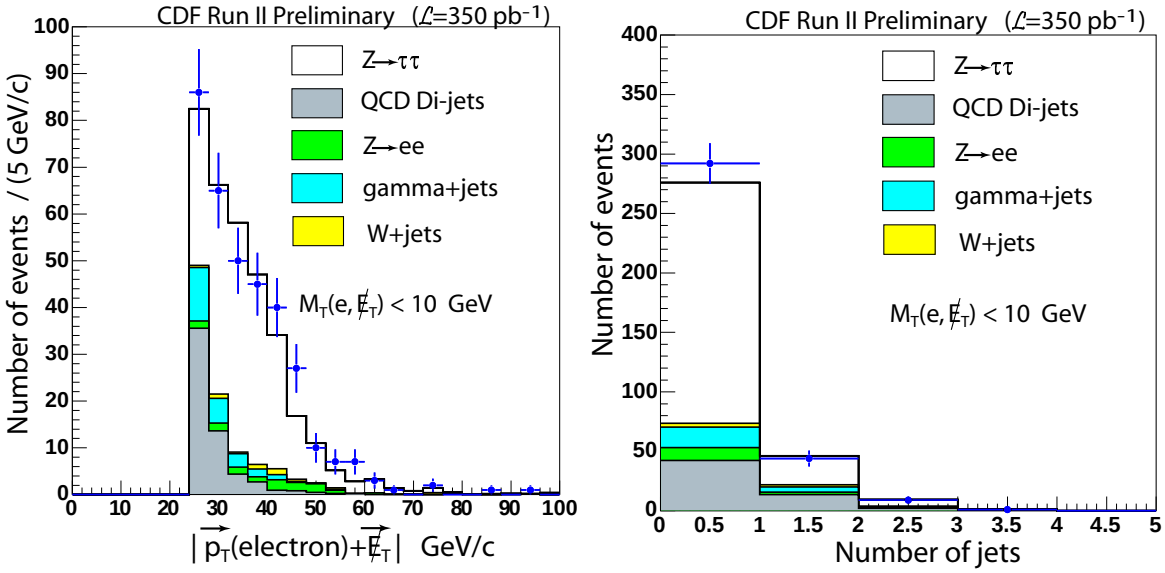

Figure 8: a) $p_T = |\vec{p}_T^{\,e} + \vec{\not{E}}_T|$ (used as an event topology cut) and b) number of jet ($E_T > 15$ GeV) distributions in "clean" signal sample of opposite-sign events obtained by applying an additional cut of $M_T < 10$ GeV.

NLO expectation of approximately 260 pb.

This measurement utilizes a novel background estimation method with accuracy exceeding all previously existing techniques, e.g. a factor of $\simeq 3-4$ over fake rate technique. In the course of performing this measurement, we established a set of tau ID cuts that are now used in most CDF analyses and defined a procedure for measuring these efficiencies using real data.

Acknowledgements

We thank members of the Tau and the W/Z Cross-Section groups for their help and support. We are very thankful to Willis Sakumoto, Eva Halkiadakis and Michael Schmitt for their help with the PDF uncertainties; Takashi Akimoto, Andrew Ivanov, Takashi Ogawa and Aron Soha for their contributions to many of the underlying studies that made this measurement possible. We also would like to thank Kathy Copic for her help with the Monte Carlo production, and electroweak conveners for many useful suggestions.

References

[1] S. Baroiant *et al.*, "Measurement of the $Z \to \tau\tau$ Cross Section Using 72 pb^{-1} of Run II Data", CDF Note 6552.

[2] S. Baroiant *et al.*, "Understanding the $Z \to \tau\tau$ Signal in Run 2 Data and Background Techniques," CDF Note 6498.

[3] S. Baroiant *et al.*, "Update on the Lepton+Track Trigger in Run II - Definition and Physics Goals," CDF Note 6325.

[4] D.Amidei *et al.*, "Measurement of $\sigma B(W \to e\nu)$, $\sigma B(Z \to ee)$ and $R = \frac{\sigma B(W \to e\nu)}{\sigma B(Z \to ee)}$ using CDF Run II Data," CDF Note 6681.

[5] C. Chen *et al.*, "Trigger and Reconstruction Efficiency for Direct Charm Mesons in the Two-Track Hadronic Data Sample", CDF Note 6165.

[6] D. Amidei *et al.*, "First Measurements of Inclusive W and Z Cross Sections from Run II of the Tevatron Collider," CDF Note 6939.

[7] S. Baroiant *et al.*, "Energy Measurement for Hadronic Taus," CDF Note 6654.

[8] E. Halkiadakis *et al.*, "PDF Uncertainties for W and Z Cross Section Measurement," CDF Note 6890.

[9] J. Insler *et al.*, "Determining the Electron Fake Rate to Hadronic Taus from the Data," CDF Note 6408.

[10] A. Soha *et al.* "Low p_T electron ID cuts and efficiencies," CDF note 7713.

[11] S. Baroiant *et al.*, "Measurement of the Electron Trigger Efficiencies for Level1 and Level2 8 GeV Triggers," CDF Note 6257; also see an update to this measurement in T. Akimoto *et al.*, "Electron Trigger Efficiency for Level1 and Level2 8 GeV Triggers," CDF Note 7710.

[12] S. Baroiant *et al.*, "Measurement of Level3 Trigger Efficiency for 8 GeV Inclusive Electron Trigger Using Conversions," CDF Note 6324.

[13] S. Baroiant *et al.*, "Measurement of Tau ID Efficiencies," CDF Note 7013.

[14] A. Anastassov *et al.*, "Search for MSSM Higgs Decaying to Taus", CDF Note 7622.

[15] S. Baroiant *et al.*, "XFT Efficiency for the Isolated Track Leg of the Electron+Track Trigger," CDF Note 6510.

[16] S. Baroiant *et al.*, "Lepton+Track Triggers: Measurement of the Level3 Trigger Efficiency for Taus," CDF Note 6553.

[17] S. Baroiant *et al.*, "γ+jet and W+jet Backgrounds to $Z/H \to \tau\tau$," CDF Note 6734.

[18] Joint Physics Group web-page.

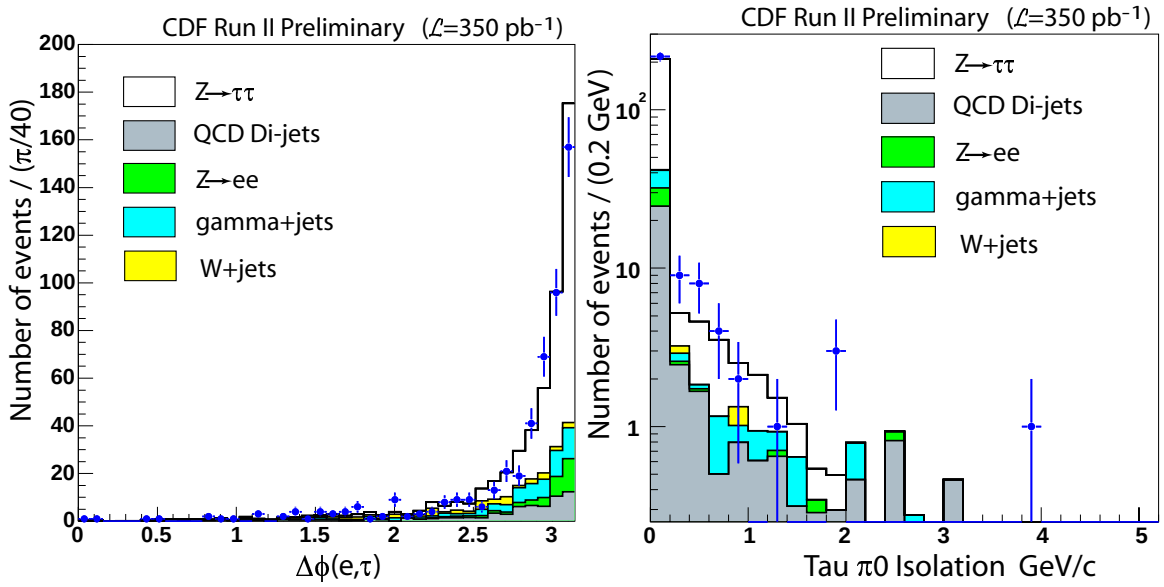

Figure 9: Distributions of a) $\Delta\phi\,(e,\tau)$ and b) π^0 isolation in the final events.

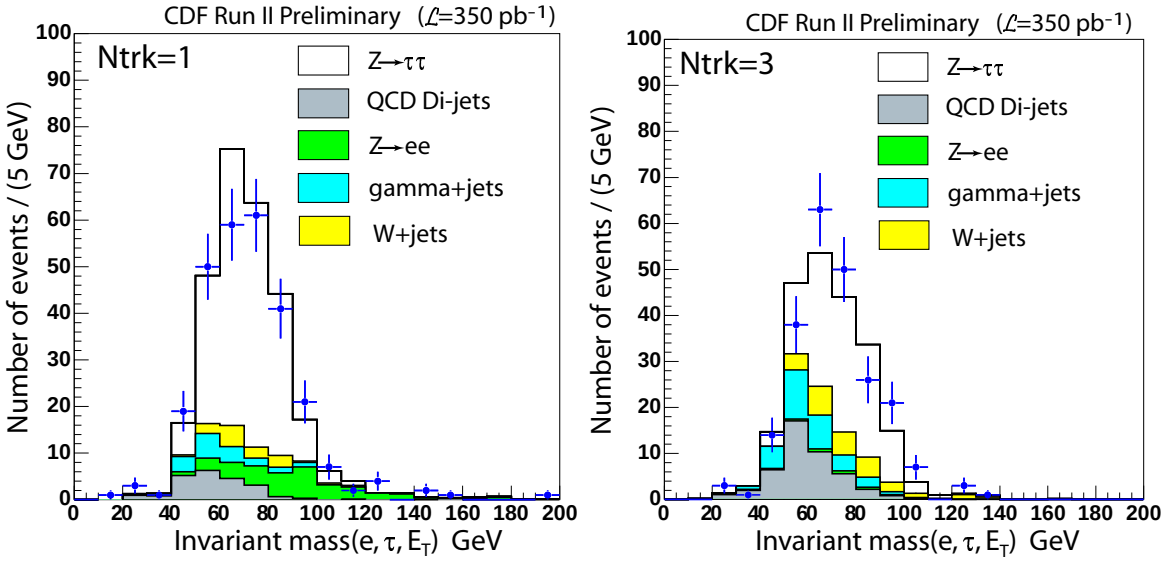

Figure 10: Distributions for the invariant mass of the electron, tau and $\not\!\!E_T$ for the final events with a) 1-prong and b) 3-prong tau candidates.

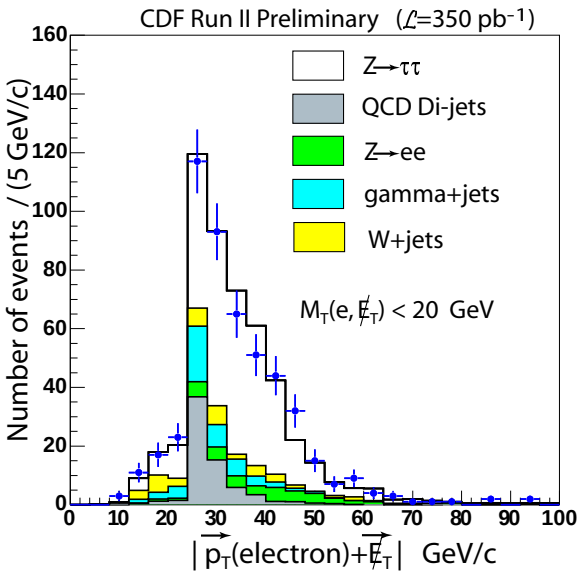

Figure 11: Distributions for the $p_T = |\vec{p}^{\,e}_T + \vec{\not{E}}_T|$ variable (used as an event topology cut) for final events passinan additional cut of $M_T < 20$ GeVdemonstrating that the yield of signal events in the low p_T region is non negligible and increases with loosening the M_T cut confirming correctness of the a priori optimization.

Appendix A

Here, we describe how we determine tau ID and isolation efficiencies. Isolation efficiency studies are also performed for

Isolation Cuts

To verify that the tau ID is reliably simulated by MC and to assign systematic uncertainties, we followed the same path as in the previous version of this analysis. We have selected a sample of $Z \to ee$ events by reversing the $\xi - cut$ on the "tau" leg and requiring that the invariant mass of the two electrons is consistent with the Z boson mass. We then selected a MC $Z \to ee$ sample using exact same cuts (including trigger simulation, although this was largely redundant as the offline cuts in all cases are tighter than the trigger requirements). We then used the electron leg to measure isolation efficiencies for the choices of track and π^0 isolations used in this analysis. Note that because there are two electrons, and fairly often both of them pass requirements for "tau" and "electron" at the same time, one can either measure the tracking efficiency "per probe leg" and "per event", thus checking not only efficiency per se, but also how accurately MC describes correlation in isolation efficiency for the two legs in the event. Comparing data and MC results under exact same selections, see Table 14, we find that the agreement is very good: for track isolation efficiency choices, the annulus N_{trk}^{10-30} and "standard" $I_{trk}^{dR<0.4}$, the numbers are typically within 1%. Note that while N_{trk} cuts is sensitive to UE only, $I_{trk}^{dR<0.4}$ cut efficiency is dominated by the amount of material via probability of emitting a photon followed by a conversion. Given that statistically all comparisons show only a borderline difference ($\simeq 2\sigma$), we choose not to correct for this difference, but rather assign a conservative estimate of 1.5% per leg on all track-related isolation efficiencies. Similar

Efficiency	"Unbiased"		"Biased"		Assigned Scale Factor
	Data	MC	Data	MC	
$N_{trk}^{10-30,\,\Delta\Theta} = 0$	79.2 ± 0.5	80.3 ± 0.2	85.8 ± 0.4	86.5 ± 0.2	1.000 ± 0.015
$I_{trk}^{e,\,\Delta R} \leq 1.0$ GeV$/c$	79.3 ± 0.5	80.5 ± 0.2	83.2 ± 0.4	84.5 ± 0.2	1.000 ± 0.015
$I_{\pi^0}^{e,\,\Delta R} \leq 0.2$ GeV$/c$	97.7 ± 0.2	98.2 ± 0.2			1.000 ± 0.010

Table 14: Comparison of isolation efficiencies measured using $Z \to ee$ data collected by lepton+track triggers.

Cut	Efficiency Data	Efficiency MC	Ratio
$N_{trk}^{10-30,\,\Delta\Theta} = 0$	81.2 ± 0.5	82.0	0.990 ± 0.006
$I_{trk}^{e,\,\Delta R} \leq 1.0$ GeV$/c$	77.6 ± 0.6	78.6	0.987 ± 0.008
$I_{\pi^0}^{e,\,\Delta R} \leq 0.2$ GeV$/c$	95.4 ± 0.2	96.5	0.989 ± 0.002
$I_{\pi^0}^{e,\,\Delta R} \leq 0.6$ GeV$/c$	96.6 ± 0.2	97.2	0.994 ± 0.002

Table 15: Comparison of isolation efficiencies measured using $Z \to ee$ data collected by an inclusive electron trigger.

agreement is observed for π^0 isolations and we assign a systematic uncertainty of 1% per leg for all π^0-related isolation efficiencies.

For further cross-checks, we used $Z \to ee$ data collected by an inclusive electron trigger, which is free of isolation biases. Our task is to measure isolation efficiency after ID cuts are applied (because this is the order of cuts in our event selection). Therefore, we select two electron candidates passing ID cuts and with the invariant mass close to the Z peak. We then calculate efficiency defined as the ratio of the number of electron candidates passing isolation requirement to the total number of electron candidates. We calculate this for each of the isolation cuts used and re-calculate the scale factor. Efficiency in data is corrected using like-sign events as an estimate of the background in the main sample. Table 15 shows the results of these calculations. Once again, we confirm that the systematic uncertainties we assign are solid.

Number of Prongs Cut

To determine the systematic uncertainty in the $N_{trk} = 1,3$ cut, we need to take into account a possibility of MC improperly simulating the rate of the UE tracks. We only care about tracks with $p_T > 1$ GeV$/c$, therefore we can use results for $N_{trk}^{10-30,\,\Delta\Theta} = 0$ cut in Table 14. Taking 80.3% efficiency for Ntrk(10-30) cut, one concludes that 19.7% of the time there is a track with pt¿1 GeV from the UE in a cone of 10-30 degrees. That corresponds to an area of size $\pi(0.52^2 - 0.17^2) = 0.7587$ in the $\eta - \phi$ space. A 10 degree signal tau cone corresponds to an area of 0.0908. Scaling areas, one obtains that 19.7%*0.091/0.759=2.36% probability to get a "random" track with $p_T > 1$ GeV inside the signal cone. If we were to repeat the same calculation using efficiency measured in data (20.8%), the probability is 2.49%. The difference is 0.13% (this is an absolute estimation for additional inefficiency in the $N_{trk} = 1,3$ cut), however each of the initial numbers (19.7% and 20.8%) have about 10% uncertainty, so the final numbers also have about 10% uncertainty (0.25% each), so we conservatively assign a 0.5% systematic error for this cut.

	Number of Reconstructed Tracks in Tau					
	1	2	3	4	5	6
Events Studied	7088	1444	3123	320	126	12
Events Failed	48	68	53	18	4	1
Cut Efficiency	0.993	0 .953	0.983	0.944	0.968	0.917
Average Efficiency	$.984 \pm .001$					
Failure Mode	Number of events					
Nuclear Interactions	33	33	29	16	3	1
K-mesons	1	13	5	1	0	0
Tau Lifetime	0	0	0	1	0	0
Conv	0	0	0	0	0	0
Pattern recognition	0	11	0	0	0	0
Other	15	11	13	2	1	0
Effic. due to "Other"	$.998 \pm .001$	$.992 \pm .003$	$.996 \pm .002$	$.994 \pm .007$	$.992 \pm .001$	1
Aver. Eff. due to Others	$0.994 \pm .001$					

Table 16: Results of the studies for lower d0 efficiency in hadonic taus. "Pattern recognition" failures denote cases when a true tau has two tracks close that are reconstructed as a single track with deviated helix parameters; "Nuclear Inetractions" mode corresponds to cases when a charged pion interacts with nuclei in the material; "Tau Lifetime" corresponds to cases when tau has decayed very far from the beamline, "Other" denotes remaining cases that should be similar to e.g. electronic decay modes.

Impact Parameter Cut for Tau Seed Track

We have studied the effects related to lower efficiency of the d_0 cut for hadronically decaying taus. We looked at the failures on event-by-event basis and comapred OBSP and reconstructed level information. We used a subsample of MC events used in the main analysis, and in addition to requirement of matching at the acceptance stage, we required that the tau tested for passing the d_0 cut is a real tau by matching tracks between reconstructed level and OBSP to exclude a (small) fraction of events when a jet is reconstructed as a tau (although this is a small effect, such occurances occasionally happen at this early stage of MC event selection).

By studying these events, we conclude that the additional inefficiency is due to nuclear interactions of pions with the material of the detector. Second effect is pattern recognition that affects only 2-prong taus and therefore has no effect on final event selection efficiency (these events are removed by the $N_{trk} = 1,3$ requirement). We don't assign any additional uncertainty to this effect as the level of uncertainty ($\leq 0.5\%$) is small compared to overall systematic uncertainty ($\simeq 3\%$ for tau ID, $\simeq 8\%$ for the overall measurement).